algorithms

MDPI

Article

Design of Selective Laser Melting (SLM) Structures: Consideration of Different Material Properties in Multiple Surface Layers Resulting from the Manufacturing in a Topology Optimization

Jan Holoch *, Sven Lenhardt, Sven Revfi and Albert Albers

IPEK—Institute of Product Engineering at Karlsruhe Institute of Technology (KIT), Kaiserstrasse 10, 76131 Karlsruhe, Germany; s.len@t-online.de (S.L.); sven.revfi@kit.edu (S.R.); sekretariat@ipek.kit.edu (A.A.)
* Correspondence: jan.holoch@kit.edu; Tel.: +49-721-608-46472

Abstract: Topology optimization offers a possibility to derive load-compliant structures. These structures tend to be complex, and conventional manufacturing offers only limited possibilities for their production. Additive manufacturing provides a remedy due to its high design freedom. However, this type of manufacturing can cause areas of different material properties in the final part. For example, in selective laser melting, three areas of different porosity can occur depending on the process parameters, the geometry of the part and the print direction, resulting in a direct interrelation between manufacturing and design. In order to address this interrelation in design finding, this contribution presents an optimization method in which the three porous areas are identified and the associated material properties are considered iteratively in a topology optimization. For this purpose, the topology optimization is interrupted in each iteration. Afterwards, the three areas as well as the material properties are determined and transferred back to the topology optimization, whereby those properties are used for the calculation of the next iteration. By using the optimization method, a design with increased volume-specific stiffness compared to a design of a standard topology optimization can be created and will be used in the future as a basis for the extension by a global strength constraint to maintain the maximum permissible stress and the minimum wall thickness.

Keywords: additive manufacturing; selective laser melting; finite element analysis; topology optimization; product development; design finding

Citation: Holoch, J.; Lenhardt, S.; Revfi, S.; Albers, A. Design of Selective Laser Melting (SLM) Structures: Consideration of Different Material Properties in Multiple Surface Layers Resulting from the Manufacturing in a Topology Optimization. *Algorithms* **2022**, *15*, 99. https://doi.org/10.3390/a15030099

Academic Editors: Andrea Serani and Riccardo Pellegrini

Received: 14 February 2022
Accepted: 17 March 2022
Published: 19 March 2022

1. Introduction

In a rapidly changing world, the demands placed on products evolve in such a way that they must be as efficient as possible and, at the same time, preserve resources. In order to save resources, high material utilization within a product is necessary, whereby a positive contribution to the climate balance in the case of parts in motion can be achieved. One possible approach to reach high material utilization is function integration [1]. Thereby, functions of several parts are integrated into one, which then fulfills these functions. As a result, connecting elements can be avoided, and, ultimately, weight is saved. However, function integration often results in multiaxial load cases which lead to complex structures and can only be partially handled with standardized tools such as design guidelines.

For this reason, CAE-based tools such as topology optimization are increasingly used. This enables the design of load-compliant structures, even under multiaxial load cases, and an optimal material distribution in a given design space [2]. One established topology optimization is the density-based approach. This approach is commonly used for single-material optimization and is covered by commercial, validated solvers but also remains an ongoing research topic. Density-based topology optimizations use the finite element method (FEM) to identify load paths in an iterative process and adjust the material

distribution in the defined design space until a given objective function is maximized or minimized. For this purpose, a fictive density $\rho[i]$ is assigned to each element i, whereby the Young modulus $E[i]$ of each element is defined as follows [3]:

$$E[i] = \rho[i]^p * E_0 \quad (1)$$

E_0 describes the Young modulus of the initial material which is defined during the initialization of the topology optimization. Furthermore, the often used SIMP approach introduces a penalty factor p which leads to a continuous material distribution. In each iteration, the fictive densities and thus the Young moduli are systematically adjusted by the optimization algorithm until a defined convergence criterion is met [3]. A common objective function, for instance, is to maximize stiffness under a given volume reduction. In density-based topology optimization, a distinction can essentially be made between two optimization approaches for satisfying the objective function. In the controller-based approach, an optimality criterion is defined. Based on this criterion, the objective function is achieved in a given number of iterations and is therefore computationally efficient. In contrast, the sensitivity-based approach bases on the calculation and evaluation of sensitivities, whereby additional restrictions such as a minimum wall thickness, a strength constraint or demolding constraints can be taken into account [4]. An algorithm employed by commercial tools to adjust sensitivities within the topology optimization represents the method of moving asymptotes (MMA) [5]. In addition to density-based topology optimizations for a single material, there are also those for multiple materials [6]. The basic approach of such a multi-material topology optimization is to minimize the compliance while taking into account two constraints: the reduction in the total volume, and the maintenance of the respective volume limits of the materials to be combined. Thereby, the materials used can be freely arranged in the design space by the optimization. Another possible approach for single-material as well as multi-material topology optimization offers the level set method and has been a steadily growing research topic in recent years [7].

However, the result of a finite element (FE)-based topology optimization causes complex structures which usually cannot be produced with conventional manufacturing or only with additional effort and thus high costs [8]. These high costs can arise from the production of special dies and become amortized only with increasing batch sizes, making individual productions or small series economically inefficient [9]. Particularly for small batch sizes, additive manufacturing (AM) provides an economical solution with which complex parts can be created. Depending on the individual case, the production can not only be more cost effective but also result in shorter cycle times and less material consumption [10]. Responsible for this is the high design freedom in AM compared to conventional manufacturing [11]. This high design freedom offers great potential for lightweight design and has moved AM more into the focus of industry and research in recent years. Current research topics are dedicated to both further developments of manufacturing and material characterization and fundamental questions such as the application scope of AM or the optimal process parameters [12]. Another research focus is the consideration of the print direction in the design of AM parts, since anisotropic and/or locally varying material properties can arise within the parts [13].

In powder-based additive manufacturing processes, powder layers are applied incrementally and melted locally by a laser beam, in order to build up a part layer by layer [14]. Thereby, it is primarily the selected process parameters such as the scan strategy or the laser power that determine the final material properties of the manufactured part [15]. Such a scan strategy that is employed in selective laser melting (SLM) is divided into two steps: first the outer contour and then the inner volume are melted in each layer [14]. This scan strategy ensures high shape fidelity of the resulting part and is therefore frequently applied [11]. However, especially at economically relevant printing rates, this scan strategy can lead to the appearance of three areas with different porosity distributions which, in turn, influence the mechanical material properties in the printed part [13]. This effect was investigated for aluminum powder in the project “SLM-Topo” funded by the DFG [16].

Thereby, the "Creator" from Coherent served as a printer for this purpose. The selected process parameters can be found in Table 1.

Table 1. Process parameters for the investigation of different porosity distributions.

Laser Power	Scanning Speed	Hatching Distance	Layer Thickness
250 W	900 mm/s	150 µm	30 µm

Figure 1 shows a sectional view (x–y plane) of the three investigated porous areas which were formed by the presented scan strategy and resulted from the used process parameters. Particularly in the so-called interface area, which occurs between the contour and hatching areas, pores appear more frequently. In comparison, there is a significantly lower number of pores in the hatching area and almost no pores in the contour area. The three areas occur exclusively in the layer planes (x–z plane) along the print direction (y-axis) (see Figure 1 left). The material properties of the AM part are thus directly dependent on its shape and the print direction.

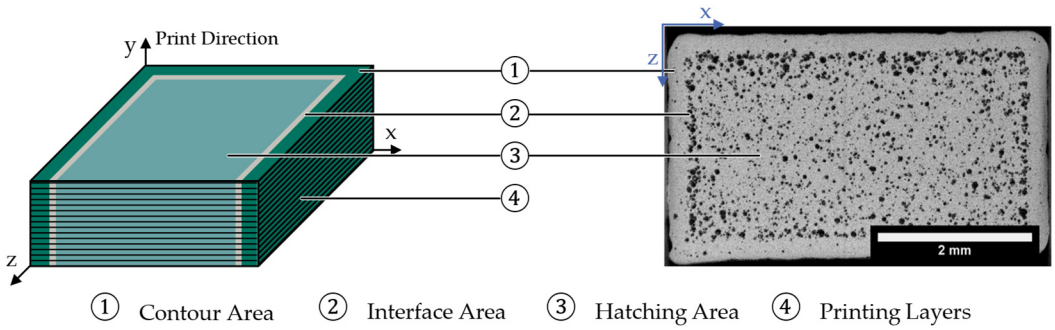

Figure 1. Exemplary representation (cut through x–y plane) of the three porous areas (**left**) and CT scan to visualize the porosity distribution in one print layer (**right**) adapted from [17].

Revfi et al. [18] investigated an interrelation between manufacturing and design using the example of fiber-reinforced polymers. Depending on the respective part shape, there are different fiber orientations due to the manufacturing which, in turn, decisively determine the arising material properties. By considering the fiber orientations in an optimization process, it was possible to generate structures specifically adapted to the load case. The consideration of process boundary conditions and their effect on material parameters directly during modeling and optimization can thus provide a decisive advantage with regard to optimal material utilization in early development phases such as design finding.

As previously described, AM is particularly suitable for the production of complex parts (e.g., the result of a topology optimization) that result due to multiaxial load cases. Considering the investigations of Revfi et al. [18], it can be assumed that the simulative consideration of the shape-dependent material properties of SLM in a topology optimization is beneficial for design finding. For this purpose, there is a need for a topology optimization that integrates the three porous areas which occur along the print direction depending on the part surface (see Figure 1 left). Since the three porous areas could be considered as three materials, a multi-material topology optimization can be considered. Due to the specific dependency of the areas on the part surface, a single-material approach is suitable as well. Such an approach based on filters for the consideration of surface coatings in a density-based topology optimization was investigated by Clausen et al. [19]. Suresh et al. [20] also analyzed, based on filters, the consideration of a surface layer resulting from the AM of metallic materials in a topology optimization. In each case, it was shown that the consideration of a surface layer, which has different material properties compared to the rest of the part, has a significant influence on the optimization result. However, the authors considered the entire surface of the component as coated and did not implement any differentiation,

for example, in the print direction, as is necessary for the investigated SLM under the given process parameters.

In order to respect the print direction of AM and its effects on the part, process simulations can be employed. Thereby, the printed paths are simulated using the G-code, and an FE model is built up element by element and linked with thermal models [21]. Thus, predictions for the resulting material properties can be made and are mainly used for the determination of emerging residual stresses. However, these coupled process simulations are computationally expensive [21]. Therefore, the iterative use within a topology optimization is not considered to be purposeful due to the high computation time.

In this contribution, an approach for the iterative consideration of shape-dependent material properties in a 3D topology optimization is presented. The three porous areas of the investigated SLM (see Figure 1) are distinguished and taken into account depending on the print direction. The optimization aims to achieve the highest possible stiffness under a given volume constraint and will be used in the future as a basis for the extension by a global strength constraint to maintain the maximum permissible stress within the three areas. The results are used to discuss the fundamental structure of the approach and the necessity of its extension. Furthermore, its potential for design finding in the product development process is analyzed.

2. Methodology

The layer-by-layer build-up of material in SLM can lead to the formation of three near-surface areas with different material properties depending on the part shape to be manufactured. As a result, there is a direct interrelation between product design and manufacturing in the product development process for SLM parts given the investigated process parameters. In order to generate a design adapted to SLM which cannot be considered intuitive due to the interrelation, computer-aided optimization methods are suitable. Therefore, these optimization methods must be adapted in order to handle the basic parameters (e.g., material properties or print direction). As shown previously, thus far, no topology optimization approach exists which takes into account three porous material areas along a given print direction. Therefore, an optimization method has been developed which iteratively considers these three areas to generate a new product design [17,22]. This contribution refers to the further development of the 3D optimization method. Due to the good availability and high robustness of commercial tools, the optimization method was developed based on Abaqus 2019 as well as Tosca 2019 and uses their solvers [23].

The basic procedure of the developed optimization method is characterized by the interruption of the topology optimization in each iteration. Then, based on the interim result obtained from the interruption, the three porous areas including the associated material properties of the SLM are determined and adopted as input parameters for further calculation in the next iteration. The procedure is repeated until a convergence criterion is reached. This creates a possibility to integrate the restrictions of the investigated SLM in a sensitivity-based topology optimization. The aim is to achieve an improved product design in terms of stiffness through the targeted, iterative manipulation of the topology optimization in comparison to a standardized topology optimization. Based on this, the method will be extended in the future to consider the maximum permissible stress in the three areas. This will be conducted by adding a global strength constraint, thus creating an advantage compared to a standard topology optimization.

The workflow of the developed optimization method is shown in Figure 2. It will be explained in the following and, at the same time, serves to structure this contribution.

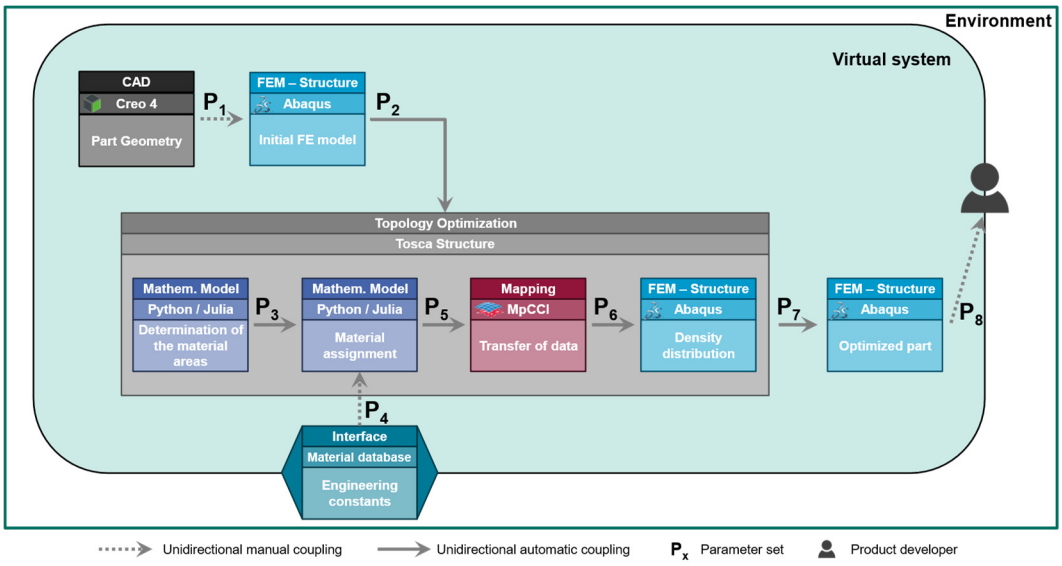

Figure 2. Workflow of the developed optimization method.

In the first step, *Part Geometry*, a part is defined that will be used in the optimization method. For this purpose, the part is derived from any CAD software, such as Creo Parametrics 4, and imported into a FE software such as Abaqus 2019. In the step *Initial FE model*, the load case including boundary conditions as well as the initial FE mesh (mesh type and size) for the topology optimization is specified and the optimization parameters are defined in the FE software. Furthermore, in this step, the material properties from the hatching area are applied to the entire part. Therefore, no differentiation into the three areas is made at this point. With this initial FE model, a sensitivity-based topology optimization is started in Tosca Structure 2019. Within this optimization, the sensitivities are calculated in Abaqus [24] and are adjusted by the MMA algorithm according to [5]. In the further progress of the method, the material properties are adapted to the material properties in the contour and interface area by manipulating the fictive densities (see step *Density distribution*).

In each iteration, the topology optimization is now interrupted right before the solver is started. During this interruption, the steps *Determination of the material areas*, *Material assignment*, *Transfer of data* and *Density distribution* are performed and represent the core of the developed optimization method. By these four steps, the three porous areas are determined, and the associated material properties are defined and passed to the topology optimization as input to calculate the next iteration. To interrupt the topology optimization, the Python interface provided by Tosca including the "hook" function is used [23]. This function enables the execution of scripts during the interruption of the optimization. In the context of the developed optimization method, scripts are executed in Python and, for computational efficiency, in Julia (see Figure 2) [25,26].

In the following, the four steps during the interruption will be explained. For the step *Determination of the material areas*, first, the surface of the part to be subdivided is needed. Therefore, during the interruption of the topology optimization, the interim result available in the interrupted iteration is exported as a smoothed surface mesh in the Standard Triangulation Language (STL) format using Tosca Structure (see Figure 3 top).

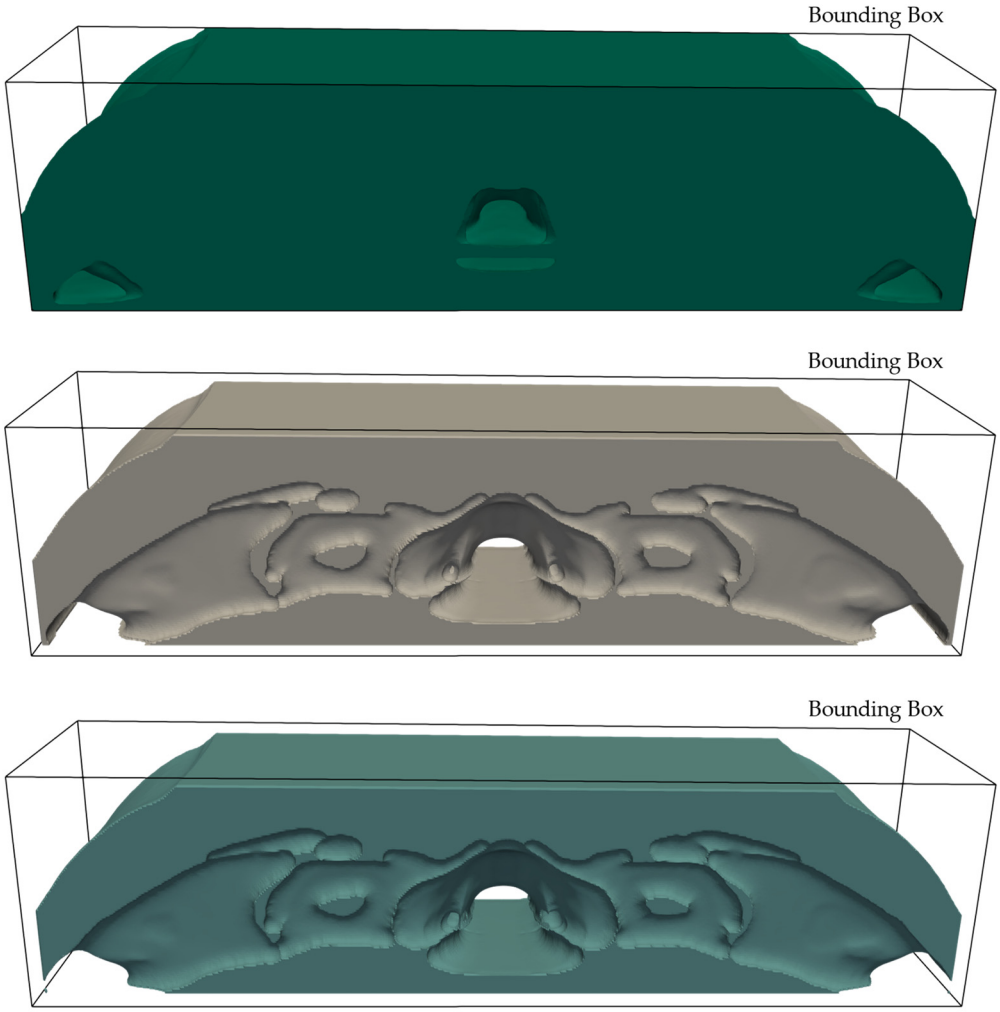

Figure 3. Surface meshes of the interim result (**top**) as well as offset 1 (**center**) and offset 2 (**bottom**).

For smoothing, the standard Tosca procedure is applied in which all elements with an iso value below 0.3 are removed [23]. At this point, 0.3 is employed, since it is the default value in Tosca and thus was taken as given. A variation of this value as well as its effect on the result has to be investigated in the future. In the very first iteration of the topology optimization, the derived surface mesh corresponds to the part defined in the *Part Geometry* step. Based on the exported surface mesh, the boundary (offset 1) between the contour and interface area (see Figure 3 center) as well as the boundary (offset 2) between the interface and hatching area (see Figure 3 bottom) is determined. These two offsets each describe the boundary between the areas with different porosities and thus enable distinguishing them from each other. To calculate the offsets, a spatial grid is created within a bounding box that describes the maximum dimensions of the exported surface mesh (see Figure 3 top). The nodes of the grid are then used to generate a signed distance field (SDF). For this purpose, the minimum distance as well as the position (inside or outside the surface mesh) of each node to the surface mesh is required [17]. The minimum distance results from the distance of the considered node to the closest triangle of the surface mesh [27]. Using the principle of winding numbers, it is possible to determine the position (inside or outside the surface mesh) of the considered node with respect to the surface mesh [28]. Once the SDF is available, the marching tetrahedra algorithm can be used to generate the two offsets (see Figure 3 center and bottom) consisting of triangles with the desired distance to the surface mesh [29].

With the surface meshes available for the interim result (see Figure 4 top), a division into the three porous areas can be performed. For this purpose, the respective regions between the surface meshes are meshed with tetrahedral elements (TE) by TetGen without changing the position of the triangles of the surface meshes, thus ensuring the conformity of the mesh [30]. As a result, each porous area is geometrically represented in the TE mesh (see Figure 4 bottom).

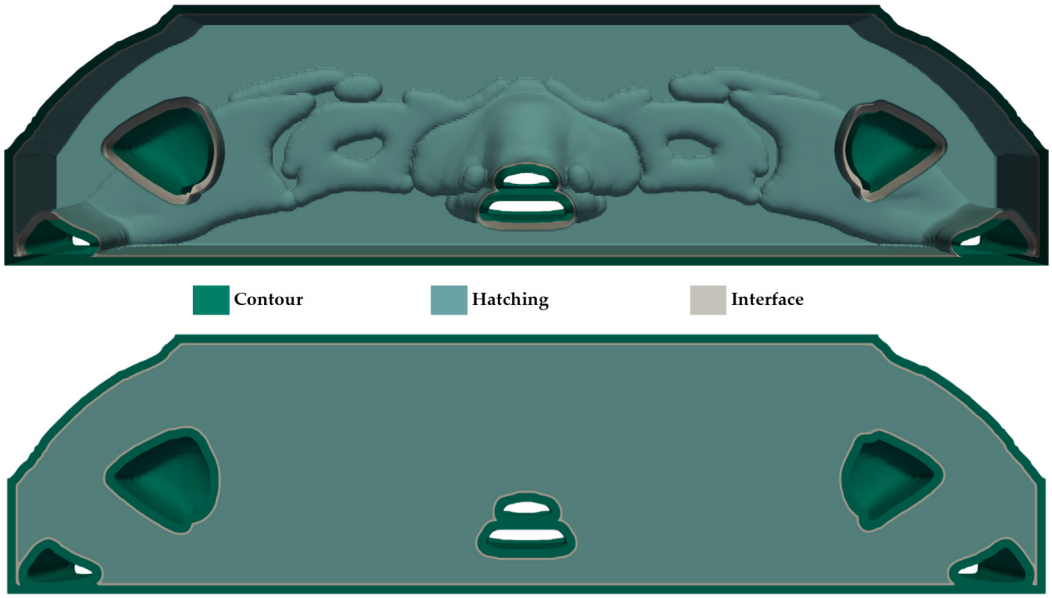

Figure 4. Surface meshes (**top**) as well as meshed areas including assigned material properties of the interim result (**bottom**).

In the *Material assignment* step, the material properties now can be automatically retrieved from a database (*Engineering constants*) and assigned to the respective elements in the three porous areas. The material properties of the three porous areas are stored in this database as engineering constants which were derived from material characterizations [31]. Due to the offset generation by means of an SDF, the three porous areas are currently present in all spatial directions (see Figure 4 bottom). Therefore, the assigned material areas are now processed in such a way that a progression as shown in Figure 1 (left) occurs and thus takes into account the SLM. It is important to note that the three porous areas are created exclusively in the layer planes (x–z plane) along the y-axis. Therefore, all TE in the contour and interface areas, which lie exactly in the respective layer planes (x–z plane), must be detected and assigned to the hatching area. To make this possible, all surface elements in the contour and interface area whose normal vectors point in the print direction (y-axis) are determined. Subsequently, the corresponding TE are derived and clustered. Finally, the material properties of the hatching area from the database are assigned to these clustered TE (see Figure 5 top).

In the *Transfer of data* step, the material properties are now transferred to the initial FE mesh of the topology optimization which is used for the FE analysis in each iteration. Therefore, the TE mesh generated in the step *Determination of the material areas* with the material properties assigned in the step *Material assignment* is transferred to the initial FE mesh of the topology optimization. The mapper software MapLib from Fraunhofer SCAI is employed for this purpose [32]. Herein, a weighted element mapping algorithm is used (see Figure 5 bottom).

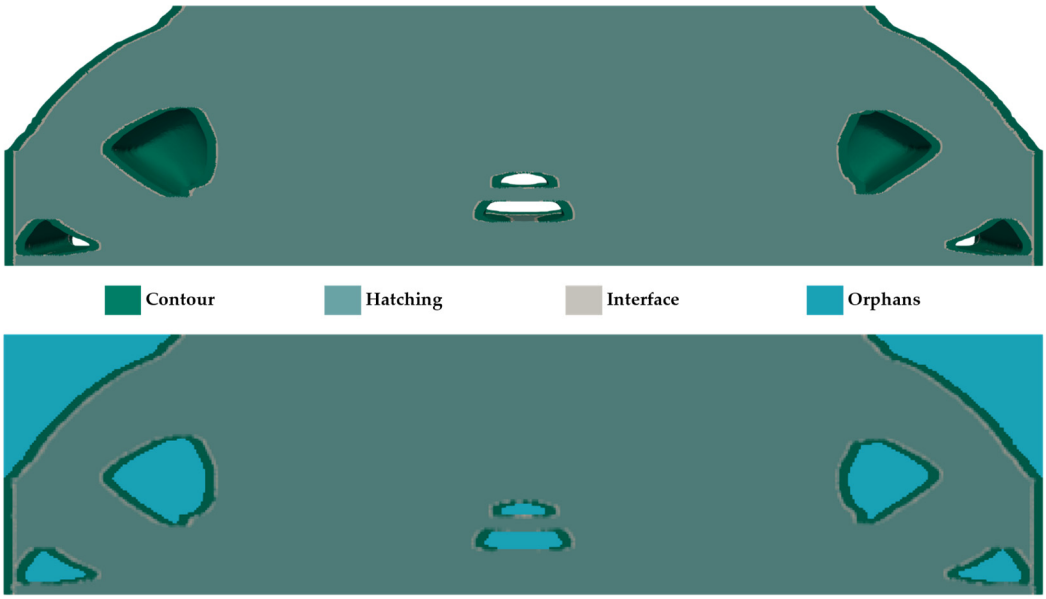

Figure 5. Porous areas including assigned material properties of the interim result considering the print direction (**top**) and material properties transferred to the initial topology optimization mesh (**bottom**).

Having determined the material properties in each element i of the initial FE mesh of the topology optimization, the fictive densities $\rho[i]$ can be adjusted in the *Density distribution* step. This adjustment is necessary as the optimization algorithm employs the fictive densities which Abaqus needs to calculate the sensitivities for the next iteration. Therefore, the Young modulus of the hatching area $E_{Hatching}$ is used as a reference value, since it has been assigned to all elements in the *Initial FE model* step. If an element in the initial FE mesh of the topology optimization has a Young modulus $E[i]$ lower than that of the hatching area due to the transferred material properties, the element is penalized by a reduction in the fictive density. If, on the other hand, the Young modulus is higher, the fictive density is increased. This results in the following equation for the fictive density $\rho_A[i]$ adjusted per element:

$$\rho_A[i] = \rho[i] * \frac{E[i]}{E_{Hatching}} \tag{2}$$

Using the SIMP approach, the scaled Young modulus $E_A[i]$ for each adjusted element is given as follows:

$$E_A[i] = \rho_A[i]^3 * E_{Hatching} = \left(\rho[i] * \frac{E[i]}{E_{Hatching}}\right)^3 * E_{Hatching} \tag{3}$$

This scaled Young modulus is now used to perform the FE analysis, based on which the sensitivities are derived by Abaqus. Subsequently, the MMA algorithm implemented in Tosca carries out the adjustment of the fictive densities for the next iteration.

These four steps consisting of *Determination of the material areas*, *Material assignment*, *Transfer of data* and *Density distribution* are applied in the topology optimization in each iteration until a convergence criterion is reached. The standard procedure used by Tosca is employed to determine convergence [33]. Thereby, the change in the objective function and the element densities is evaluated after each iteration. If the change in the objective function is less than 0.001 and that in the element densities is less than 0.005 compared to the last iteration, convergence can be assumed.

The result of the developed optimization method is an optimized product design (*Optimized part*) which considers the three porous areas of the SLM.

3. Model Design

To investigate the application of the developed optimization method and its effects on the resulting design, a three-point bending beam is used as an example load case. The example is intentionally kept simple because the contribution is focused on the method and its evaluation in the context of design finding. Therefore, a simple example helps to evaluate the plausibility of the results. The bending beam is clamped in a fixed-loose bearing at the bottom side edges and centrally loaded with a displacement d of 0.24 mm (2% of the maximum height) (see Figure 6). The sensitivity-based optimization approach, described in the previous chapter, is applied. Through the usage of such a sensitivity-based approach, the possibility is offered to consider additional boundary conditions in the future, such as a minimum wall thickness or a global strength constraint [17]. This is intended by the authors as a further development as well as an improvement of the optimization method and will be discussed in the following.

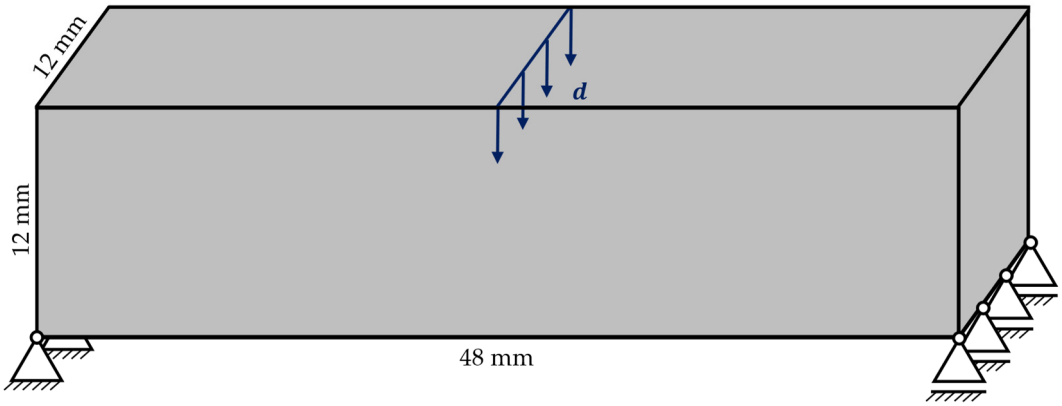

Figure 6. Three-point bending beam with dimensions, clamping and loading.

The material properties (Young's modulus and Poisson's ratio) for the three porous areas which arise due to the chosen process parameters were characterized in material testing (see Table 2). For this purpose, in addition to CT analyses for detecting the porosity distribution, ultrasonic phase spectroscopy (UPS) and resonant ultrasound spectroscopy (RUS) were employed for the determination of the mechanical material properties [31]. The chosen material for characterization is AlSi10Mg. In addition to the material properties, Table 2 also shows the thicknesses of the areas as they appear in the SLM in each layer plane. No explicit thickness is defined for the hatching area, since this results from the total volume without the contour and interface areas and thus always describes the remaining inner area (see Figure 1 left).

Table 2. Dimensions and material properties of the three porous areas.

	Contour Area	Interface Area	Hatching Area
Young's modulus [GPa]	75	65.5	72.5
Poisson's ratio [–]	0.35	0.35	0.35
Thickness [mm]	0.4	0.1	-

In order to model each layer within the optimization method despite the small thickness, the global element edge length must not exceed the thickness of the interface area. Therefore, in this contribution, a global element edge length of 0.1 mm is defined. Hexahedral elements are applied as the element type, since, in comparison to tetrahedral elements, they do not have an artificial stiffening effect. Due to the lower computation time, a linear shape function is chosen. These chosen parameters result in a mesh consisting of 6.9 million

hexahedral elements. By exploiting the symmetry of the load case, the number of elements can be halved and the calculation time accelerated. The overall goal is the maximization of the stiffness. Therefore, as the objective function of the optimization, maximizing the strain energy under a given volume reduction to a relative final volume of 60% is defined. Thus, the goal is a structure that retains as much internal energy as possible to withstand the defined deformation.

In order to evaluate the resulting design from the presented optimization method both qualitatively and quantitatively, it is compared to the design from a standard topology optimization performed with only one set of material properties. For this evaluation, a static FE analysis based on the same FE model (e.g., the initial topology optimization mesh defined in *Initial FE model*) is performed. Therefore, for each of the two designs (resulting from the developed optimization method and the standard topology optimization), the three porous areas and thus their material properties are transferred to the FE model. For this purpose, the three porous areas are identified for both designs, and the respective E-moduli are mapped onto the FE model. The procedure here corresponds to the first three steps of the interruption (see Figure 2). This allows a comparison of the strain energy as well as maximum stresses of the two final designs resulting from the optimizations under the same conditions [17].

4. Results and Discussion

In the following, the results are presented and discussed, which were obtained using the developed optimization method (see Figure 7) and a standard topology optimization (see Figure 8).

Figure 7. Result of the developed optimization method: overall design (**left**) and sectional view (**right**).

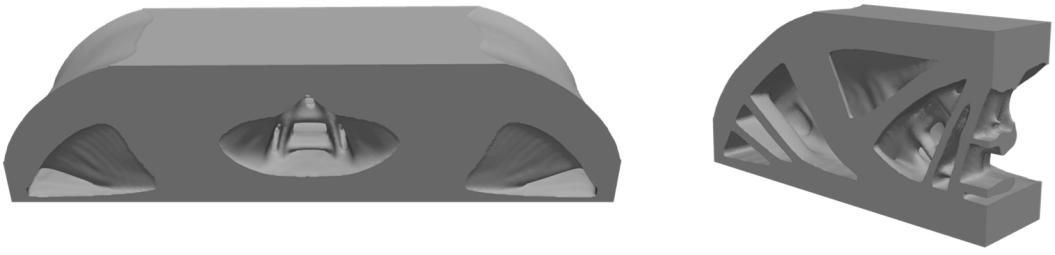

Figure 8. Result of the standard topology optimization: overall design (**left**) and sectional view (**right**).

If the results are considered qualitatively, it can be stated that both optimizations form a type of truss structure consisting of struts along the main load paths. This can be explained by the defined three-point bending load case. However, a closer look reveals clear differences. The standard topology optimization (see Figure 8 left) results in wide indentations in the lower corners and a large hole in the middle of the beam. In contrast, the developed optimization method (see Figure 7 left) results in both the indentations and the hole being much smaller. Instead, a type of hollow structure is created which is illustrated by the sectional view (see Figure 7 right). Furthermore, the results indicate that the developed optimization method tends to an increased number of thin struts compared

to the standard topology optimization, as can be seen, for example, in the corner of the clamping based on the three struts. This leads to the assumption that the developed optimization method maximizes the contour area of the resulting design. The assumption can be confirmed by the quantitative evaluation of the contour area, since the design of the developed optimization method has an approximately 7% bigger contour area compared to the design of the standard topology optimization (see Table 3). To obtain this quantitative evaluation, all hexahedral elements which have the material properties of the contour area are determined. The number of elements recorded this way allows the volume of the contour area to be estimated, since all hexahedral elements have the same size due to the simple geometry of the bending beam. The effect of the contour area maximization could be triggered due to two factors. Firstly, beginning with the first iteration, the three porous areas are considered in the FE model, and thus the outer surface (contour area) is improved along the print direction in the initial FE model. This leads to the assumption that the optimization algorithm thus does not eliminate the improved elements, resulting in the hollow structure. However, by observing the interior of the beam, it can be shown that the surface area is also increased there. Thus, the influence due to the consideration of the three porous areas from the first iteration onwards is estimated as small. Rather, the increase in surface area can be explained by the second factor, the material properties from Table 2. The Young modulus in the contour area is the highest and thus also has the highest material stiffness. This increased stiffness is preferred by the optimization algorithm and leads to a bigger contour area. This result allows the assumption that the described procedure within the developed optimization method can be classified as plausible and purposeful.

Table 3. Quantitative evaluation of the two resulting designs.

	Developed Optimization Method	**Standard Topology Optimization**
Final volume [%]	65.83	65.69
Strain energy [mJ]	350.247	348.598
Required iterations [–]	39	37
Contour/Interface/Hatching area [%]	37.77/7.68/54.55	30.86/7.58/61.56

In addition to the qualitative evaluation, it is important to perform a quantitative analysis as well. Therefore, a static FE analysis, in which the three porous areas including the material properties are transferred to the resulting designs, was performed and the strain energy calculated. Furthermore, the actual final volume as well as the required iterations was extracted. The resulting values are presented in Table 3.

The developed optimization method leads to an increasing stiffness by extending the contour area. Therefore, the volume-specific strain energy $\left[\frac{\mathrm{mJ}}{\mathrm{mm}^3}\right]$ is evaluated which results in an approximately 1% higher value for the design of the developed optimization method. From this analysis as well as the qualitative evaluation, it can be concluded that the developed optimization method produces a visually modified design which also leads to a slightly increased stiffness for the same volume due to the targeted redistribution of material. Therefore, the quantitative evaluation supports the assumption already made on the basis of the qualitative results that the described procedure is plausible and purposeful even with the increased stiffness of only 1% under the given parameters and load case.

In order to examine the optimization history in addition to the final results, the progression of compliance up to convergence was analyzed (see Figure 9).

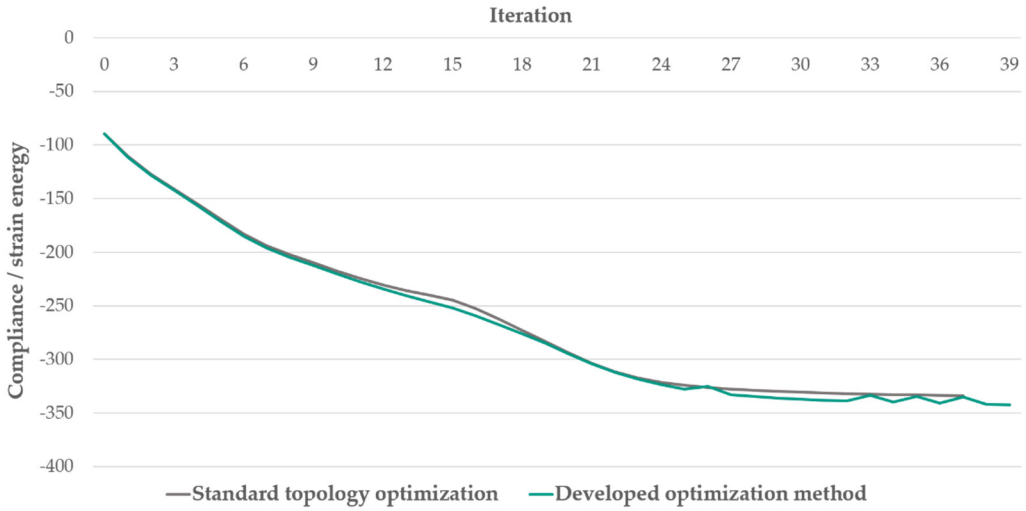

Figure 9. Comparison of the optimization history of the standard topology optimization and the developed optimization method.

It is noticeable that both the standard topology optimization and the developed optimization method have a very similar optimization history, and no divergence or severe discontinuities in the compliance are generated by adjusting the fictive densities. Furthermore, it can be seen that approximately the same number of iterations are required to generate the two very different designs. The observation of the optimization history thus allows the assumption that no significant disturbance in the convergence is introduced by the adjustment of the fictive densities, whereby the developed optimization method also generates an optimized design in a targeted manner.

Therefore, the assumption is made that the presented optimization method can be used as a basis for extensions. In the following, based on the results of a stress analysis and by examining the final design, the necessary and plausible extensions of the presented optimization method are discussed.

In addition to the findings regarding the volume-specific stiffness, the static FE analysis can be used to analyze the prevailing stresses. Here, 230 MPa was defined as the critical stress, since this can be assumed to be the yield stress and thus the limit of plastic deformation for the applied material. All elements exceeding this stress value are colored gray in Figures 10 and 11 right. It can be seen that especially the load application and the clamping regions exceed the value of 230 MPa. Furthermore, the elements at the bottom of the two beams, where a high stress due to bending is present, exceed 230 MPa. This follows primarily from the load itself and is mainly due to the selected displacement d. This displacement was chosen arbitrarily, since its value for an optimization purely for stiffness has no influence on the result. Rather, it is intended to show, on the basis of the stress evaluation, that an abrupt stress progression occurs across the porous areas (see black marking in Figures 10 and 11 right) which is caused by their different Young moduli. The contour area exhibits the highest stress and the interface area the lowest. This correlates with the Young modulus, since the higher Young modulus causes a higher stress at the same load. If the limit of 230 MPa is now applied, it is possible that this limit will not be exceeded in a standard topology optimization in which the three porous areas are not taken into account. However, if the porous areas from the SLM are subsequently transferred to the design and evaluated in a static FE analysis, the critical stress of 230 MPa may be exceeded due to the higher Young modulus in the contour area. Therefore, it is obvious that this critical stress should already be taken into account directly in the optimization method. This can be conducted, for example, by defining a global strength constraint. The optimization method presented provides a possible basis for implementing such a global strength constraint and can thus help to ensure that the maximum allowable stresses are

not exceeded in the three porous areas. Such an implementation is temporarily under investigation.

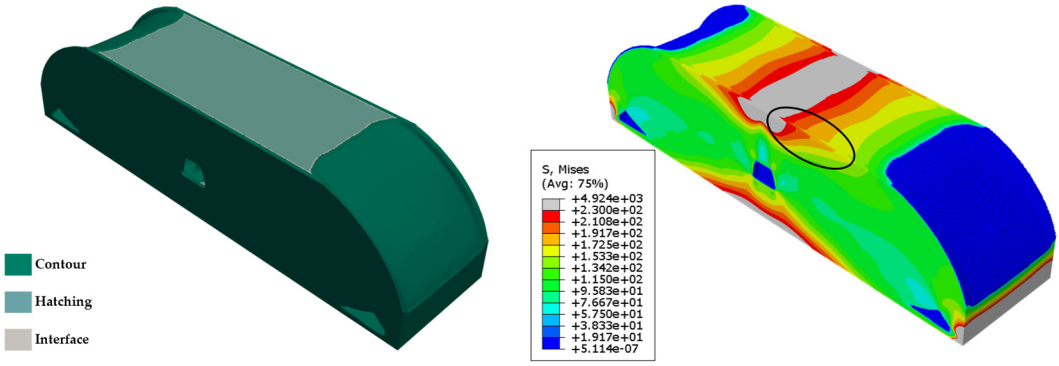

Figure 10. Resulting design of the developed optimization method including porous areas (**left**) and result of the static FE analysis (**right**).

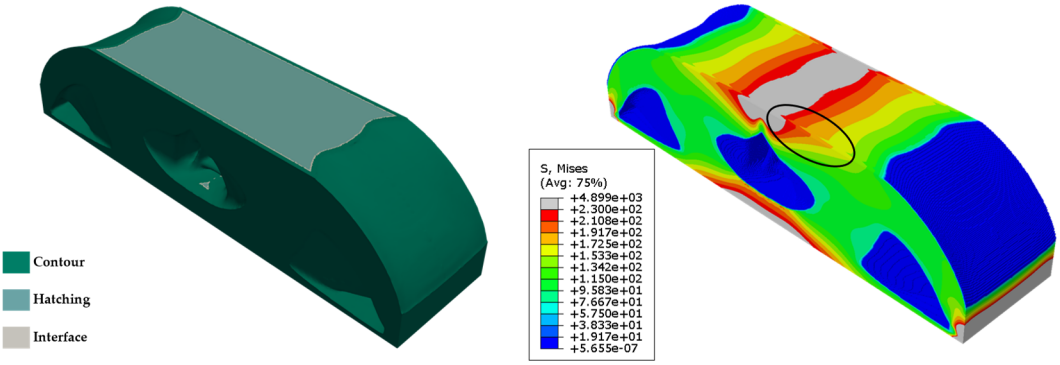

Figure 11. Resulting design of the standard topology optimization including porous areas (**left**) and result of the static FE analysis (**right**).

On the basis of a section in the layer plane, the determination of the three porous areas including material assignment is analyzed and discussed in the following. For this purpose, a section through the center (half of the total height) of the beam is used (see Figure 12). The sectional view shows that the generation of the offsets including the definition of the material areas in the *Determination of the material areas* step is generally performed correctly and that there are no overlaps between the areas. This leads to the assumption that the presented approach for the determination of the three porous areas is target-oriented. Especially in the thicker struts of the beam, the material distribution as it results in the SLM is visible and corresponds to the known distribution from Figure 1 (left). However, it is noticeable that due to the lack of restrictions in the thinner regions, not all three porous areas are represented as they appear in the SLM under the given process parameters. For example, in the hollow structure (see black marking in Figure 12), only the contour area is present and thus does not fully reflect reality. It is therefore necessary to extend the optimization method in such a way that no structures (e.g., struts) are created which are thinner than a minimum thickness. This minimum thickness results from the individual thicknesses of the material areas, since in a closed structure, the contour and interface areas as well as some hatching area must always be present twice per layer plane. Based on Table 2, this results in a minimum thickness of >1 mm. The restriction of a minimum wall thickness can be used for this purpose in the developed optimization method. This was basically studied in [17] and will be incorporated into the optimization method in the future.

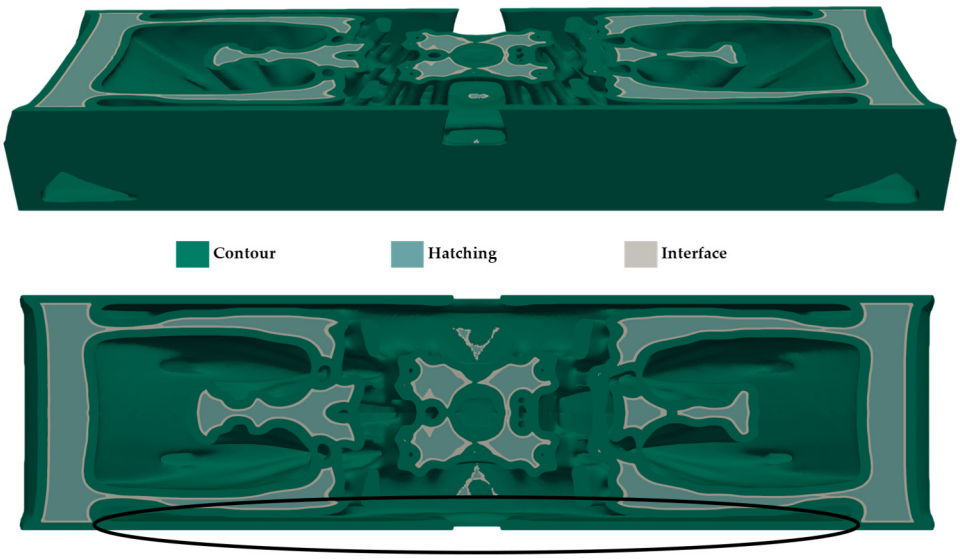

Figure 12. Section in the layer plane through the design from the developed optimization method: front view (**top**) and plan view (**bottom**).

5. Conclusions and Outlook

The integration of several functions in one part is a possible approach for saving material and thus weight. However, this often results in complex structures that cannot usually be derived intuitively. This can be remedied by computer-aided tools such as topology optimization which provide a design proposal for the part based on a given load case. In order to manufacture these parts very close to the result of the topology optimization, AM presents a potential solution. This is due to the high design freedom as well as the omitted manufacturing costs for complex tools such as dies. However, AM entails special characteristics regarding the material properties resulting from the manufacturing. In SLM, for example, three porous areas can be created in the layer planes along the print direction depending on the shape of the part and the given process parameters. These porous areas also influence the material properties in the resulting part. As a result, there is a direct interrelation between the manufacturing and the design of the part.

This contribution presents an optimization method which considers the three porous areas and the associated material properties during a sensitivity-based topology optimization in Tosca Structure. For this purpose, the topology optimization is interrupted in each iteration after the fictive density distribution has been determined and the smoothed interim result is exported. Subsequently, the three porous areas including the material properties are determined, adopted in the interim result and passed back to the optimization. Thereby, the sensitivities are calculated by Abaqus, and the implemented MMA algorithm implemented in Tosca carries out the adjustment of the fictive densities for the next iteration. As soon as the convergence criterion is reached, a design is available which is generated on the basis of the material properties resulting from the SLM under the given process parameters. From the investigations of the optimization method based on a three-point bending beam, it can be concluded that by iteratively interrupting and adjusting the material properties, a design is generated which, compared to a standard topology optimization, has an increased contour area and tends to favor thin structures. As a result, a slightly higher volume-specific stiffness can be achieved under the given boundary conditions for the three-point bending beam compared to the design of the standard topology optimization. Thus, the optimization method can contribute to the design finding in early phases of product development and offers a basis for further extensions.

Such extensions are necessary since the results show that the topology optimization results can lead to structures that do not include all three porous areas everywhere and

thus do not completely represent reality correctly. By using a minimum wall thickness in the optimization method, the possibility should be created to better represent the three porous area and thus the reality more closely in the future. In addition, the division into the areas results in an abrupt stress progression which could lead to an overestimation of the damage limits, especially in a standard topology optimization. In order to prevent such a potential overestimation, a global strength constraint shall be considered in the developed optimization method in the future. In further investigations, which are not focused in this contribution, the comparison between simulation and experiment will be established. For this purpose, the resulting designs from the developed optimization method as well as a standard topology optimization will be manufactured, characterized and investigated on a test bench.

Author Contributions: Conceptualization, J.H. and S.L.; methodology, J.H., S.R. and A.A.; software, J.H. and S.L.; writing—original draft preparation, J.H. and S.L.; writing—review and editing, J.H. and S.R.; visualization, S.L.; supervision, A.A.; funding acquisition, A.A. All authors have read and agreed to the published version of the manuscript.

Funding: The research documented in this manuscript has been funded by the German Research Foundation (DFG) within the project "SLM-Topo: Development of a process specific topology optimization method for additive manufacturing of lightweight structures exemplified by the SLM process", grant number 399233791. The support from the German Research Foundation (DFG) is gratefully acknowledged. We acknowledge support by the KIT-Publication Fund of the Karlsruhe Institute of Technology.

Institutional Review Board Statement: Not applicable.

Informed Consent Statement: Not applicable.

Data Availability Statement: The data that support the findings of this manuscript are available from the corresponding author upon reasonable request.

Conflicts of Interest: The authors declare no conflict of interest.

References

1. Albers, A.; Burkardt, N. Systemleichtbau-ganzheitliche Gewichtsreduzierung. In *Handbuch Leichtbau: Methoden, Werkstoffe, Fertigung*, 2nd ed.; Frank Henning, E.M., Ed.; Carl Hanser Verlag GmbH & Co. KG: Munich, Germany, 2020; pp. 113–132.
2. Bendsøe, M.P.; Sigmund, O. *Topology Optimization*; Springer: Berlin/Heidelberg, Germany, 2004.
3. Bendsøe, M.P. Optimal shape design as a material distribution problem. *Struct. Optim.* **1989**, *1*, 193–202. [CrossRef]
4. Dassault Systèmes. SIMULIA User Assistance 2017: Controller-Versus Sensitivity-Based Topology Optimization. Available online: https://abaqus-docs.mit.edu/2017/English/TsoUserMap/tso-c-user-TopOpt-OptTask-ContrVSSens.htm (accessed on 19 January 2022).
5. Svanberg, K. The method of moving asymptotes—A new method for structural optimization. *Int. J. Numer. Meth. Engng.* **1987**, *24*, 359–373. [CrossRef]
6. Gibiansky, L.V.; Sigmund, O. Multiphase composites with extremal bulk modulus. *J. Mech. Phys. Solids* **2000**, *48*, 461–498. [CrossRef]
7. Wang, M.Y.; Wang, X.; Guo, D. A level set method for structural topology optimization. *Comput. Methods Appl. Mech. Eng.* **2003**, *192*, 227–246. [CrossRef]
8. Harzheim, L. *Strukturoptimierung: Grundlagen und Anwendungen*; Verlag Europa-Lehrmittel: Haan-Gruiten, Germany, 2014.
9. Universität Stuttgart. Product Development with Rapid Manufacturing (PDrapid). Available online: https://www.iktd.uni-stuttgart.de/forschung/mpe/pdrapid/ (accessed on 19 January 2022).
10. Thompson, M.K.; Moroni, G.; Vaneker, T.; Fadel, G.; Campbell, R.I.; Gibson, I.; Bernard, A.; Schulz, J.; Graf, P.; Ahuja, B.; et al. Design for Additive Manufacturing: Trends, opportunities, considerations, and constraints. *CIRP Ann.* **2016**, *65*, 737–760. [CrossRef]
11. Gebhardt, A. *Additive Fertigungsverfahren: Additive Manufacturing und 3D-Drucken für Prototyping—Tooling—Produktion*; Carl Hanser Verlag GmbH & Co. KG: Munich, Germany, 2016.
12. Zhang, P.; Liu, J.; To, A.C. Role of anisotropic properties on topology optimization of additive manufactured load bearing structures. *Scr. Mater.* **2017**, *135*, 148–152. [CrossRef]
13. Kruth, J.-P.; Badrossamay, M.; Yasa, E.; Deckers, J.; Thijs, L.; van Humbeeck, J. Part and material properties in selective laser melting of metals. In Proceedings of the 16th International Symposium on Electromachining (ISEM XVI), Shanghai, China, 19–23 April 2010; Shanghai Jiao Tong University Press: Shanghai, China, 2010.

14. Gu, D.D.; Meiners, W.; Wissenbach, K.; Poprawe, R. Laser additive manufacturing of metallic components: Materials, processes and mechanisms. *Int. Mater. Rev.* **2012**, *57*, 133–164. [CrossRef]
15. Aboulkhair, N.T.; Everitt, N.M.; Ashcroft, I.; Tuck, C. Reducing porosity in AlSi10Mg parts processed by selective laser melting. *Addit. Manuf.* **2014**, *1*, 77–86. [CrossRef]
16. Holoch, J.; Czink, S.; Spadinger, M.; Dietrich, S.; Schulze, V.; Albers, A. SLM-Topo—Prozessspezifische Topologieoptimierungsmethode für im Selektiven Laserschmelzen gefertigte Leichtbaustrukturen. *Ind. 4.0 Manag.* **2020**, *4*, 45–49.
17. Holoch, J.; Lenhardt, S.; Renz, R.; Albers, A. Investigation on the influence of different modelling of multiple surface layers on a 3D topology optimization. In Proceedings of the NAFEMS World Congress 2021, Salzburg, Austria, 25–29 October 2021.
18. Revfi, S.; Mikus, M.; Behdinan, K.; Albers, A. Bead optimization in long fiber reinforced polymer structures: Consideration of anisotropic material properties resulting from the manufacturing process. *Adv. Eng. Softw.* **2020**, *149*, 102891. [CrossRef]
19. Clausen, A.; Aage, N.; Sigmund, O. Topology optimization of coated structures and material interface problems. *Comput. Methods Appl. Mech. Eng.* **2015**, *290*, 524–541. [CrossRef]
20. Suresh, S.; Thore, C.-J.; Torstenfelt, B.; Klarbring, A. Topology optimization accounting for surface layer effects. *Struct. Optim.* **2020**, *62*, 3009–3019. [CrossRef]
21. Thorborg, J.; Esser, P.; Bayat, M. Thermomechanical modeling of additively manufactured structural parts—different approaches on the macroscale. *IOP Conf. Ser. Mater. Sci. Eng.* **2020**, *861*, 12008. [CrossRef]
22. Holoch, J.; Träger, L.; Albers, A. SLM-Topo—Einfluss unterschiedlicher Modellierung von Randschicht und innerem Volumen auf eine 2D-Topologieoptimierung. In Proceedings of the NAFEMS Virtuelle DACH Konferenz 2020, Online, 13–14 October 2020; pp. 106–109.
23. Dassault Systèmes. SIMULIA User Assistance 2017: Topology Optimization. Available online: https://abaqus-docs.mit.edu/2017/English/DSSIMULIA_Established.htm (accessed on 10 July 2021).
24. Dassault Systèmes. SIMULIA User Assistance 2017: Design Sensitivity Analysis. Available online: https://abaqus-docs.mit.edu/2017/English/SIMACAEANLRefMap/simaanl-c-dsa.htm (accessed on 4 March 2022).
25. Bezanson, J.; Edelman, A.; Karpinski, S.; Shah, V.B. Julia: A Fresh Approach to Numerical Computing. *SIAM Rev.* **2017**, *59*, 65–98. [CrossRef]
26. Python Software Foundation. The Python Language Reference. Available online: https://docs.python.org/3.7 (accessed on 15 March 2021).
27. Ericson, C. *Real-Time Collision Detection*; Elsevier Morgan Kaufmann: Amsterdam, The Netherlands, 2008.
28. Jacobson, A.; Kavan, L.; Sorkine-Hornung, O. Robust inside-outside segmentation using generalized winding numbers. *ACM Trans. Graph.* **2013**, *32*, 1–12. [CrossRef]
29. Carneiro, B.; Silva, C.; Kaufman, A. Tetra-Cubes: An algorithm to generate 3D isosurfaces based upon tetrahedra. In Proceedings of the IX Brazilian Symposium on Computer Graphics, Image Processing and Vision, Los Alamitos, CA, USA, 1996; Available online: https://www.visgraf.impa.br/sibgrapi96/trabs/pdf/a26.pdf (accessed on 15 January 2022).
30. Si, H. TetGen: A Quality Tetrahedral Mesh Generator and 3D Delaunay Triangulator. Available online: http://wias-berlin.de/software/tetgen/1.5/doc/manual/manual.pdf (accessed on 18 March 2021).
31. Czink, S.; Holoch, J. SLM-Topo: Topology Optimisation Designed for Laser Based Additive Manufacturing. Available online: https://sourceforge.net/projects/slm-topo/ (accessed on 4 March 2022).
32. Spiess, H.; Oeckerath, A.; Landvogt, B. *MapLib Manual: Version 2013.0*; Fraunhofer Institute for Algorithms and Scientific Computing (SCAI): Sankt Augustin, Germany, 2018.
33. Dassault Systèmes. SIMULIA User Assistance 2020. Available online: http://scclic5.scc.kit.edu/v2020/english/dssimulia_established.htm?show=TsoUserMap/tso-c-user-TopOpt-StopCond-ConvCrit.htm (accessed on 2 March 2022).